

Magnetization and EPR studies of the single molecule magnet Ni_4 with integrated sensors

G. de Loubens,¹ G. D. Chaves-O'Flynn,¹ A. D. Kent,¹ C. Ramsey,² E. del Barco,² C. Beedle,³ and D. N. Hendrickson³

¹*Department of Physics, New York University, 4 Washington Place, New York, New York 10003, USA*

²*Physics Department, University of Central Florida,*

4000 Central Florida Boulevard, Orlando, Florida 32816-2385, USA

³*Department of Chemistry and Biochemistry, University of California San Diego, La Jolla, California 92093-0358, USA*

(Dated: January 3, 2022)

Integrated magnetic sensors that allow simultaneous EPR and magnetization measurements have been developed to study single molecule magnets. A high frequency microstrip resonator has been integrated with a micro-Hall effect magnetometer. EPR spectroscopy is used to determine the energy splitting between the low lying spin-states of a Ni_4 single crystal, with an $S = 4$ ground state, as a function of applied fields, both longitudinal and transverse to the easy axis at 0.4 K. Concurrent magnetization measurements show changes in spin-population associated with microwave absorption. Such studies enable determination of the energy relaxation time of the spin system.

An understanding of decoherence and energy relaxation mechanisms in single molecule magnets (SMMs) is both of fundamental interest [1] and important for the use of SMMs in quantum computing [2]. Quantum tunneling of magnetization (QTM) has been widely studied in SMMs [3, 4, 5]. A recent focus is on coherent QTM in which the tunneling rates may be faster than the rate of decoherence [6, 7]. Experiments on SMMs [7] and doped antiferromagnetic rings [8, 9] have been reported. However, the basic relaxation mechanisms in SMMs are still under active investigation both experimentally and theoretically [10].

We have developed sensors allowing simultaneous EPR and magnetization measurements at low temperatures (typically below 1 K) to study SMMs. A microstrip resonator [11] with resonance frequency between 25 and 30 GHz has been integrated on a chip with a micro-Hall effect magnetometer [12]. The high filling factor in such resonators allows measurement of photon absorption in very small crystals as well as the application of large microwave magnetic fields, needed for Rabi experiments. The fast response of the Hall sensor (> 1 MHz) also enables time-resolved measurements of the magnetization.

In this paper we show EPR spectroscopy of the two lowest energy levels associated with high spin states ($S = 4$) of a Ni_4 single crystal. We present simultaneous measurements of associated photon-induced changes in the magnetization. This represents an important advance from the experiments in refs. [7, 8], in which only photon induced magnetization changes were measured, and EPR studies were not possible. In particular, it enables a direct determination of the energy relaxation time of the spin system.

A schematic of our integrated sensor is presented in Fig. 1. The Hall sensor is fabricated from a GaAs/AlGaAs heterostructure 2D electron gas to form a cross of width $50 \mu\text{m}$, chosen to optimize the coupling with a SMM crystal with lateral dimensions of about $100 \mu\text{m}$. Our magnetometer has a Hall coefficient of

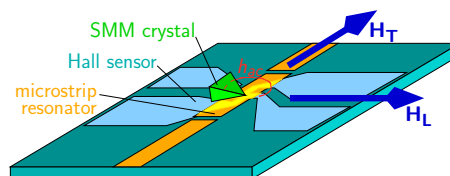


Figure 1: Schematic of the sensor developed for this study.

$1780 \Omega/\text{T}$ and a noise level of $2 \mu\text{T}/\sqrt{Hz}$ with a current of $10 \mu\text{A}$. This permits detection of changes in the magnetization smaller than 5×10^{-4} of the saturation magnetization of our SMM crystals ($\approx 5 \times 10^5 \mu\text{m}^3$), using a lock-in detection bandwidth of 300 ms. The microstrip resonator, a 250 nm thick gold line, is evaporated on top of the Hall sensor and capacitively coupled to two feedlines, so that it can work in transmission mode. It is designed to be matched to 50Ω and its fundamental resonance frequency ranges between 25 and 30 GHz ($\approx 0.4 \text{ mm}$ width and 1.5 mm length). The MW field, h_{ac} , is maximum and uniform above its center, aligned with the Hall cross. The strength of h_{ac} at the sample location was calibrated for each integrated sensor used: the circularly polarized saturation amplitude of DPPH ($h_{ac} = 0.9 \pm 0.05 \text{ Oe}$) corresponds to an incident power P_{in} of about 50 mW . This value depends on the quality factor of the resonator, found to be about 20.

The sensor is in a ^3He cryostat with a base temperature of 0.35 K . The two ports of the microstrip are connected through coaxial lines to an Agilent PNA 50 GHz vector network analyzer with copper and stainless steel sections to minimize thermal and MW losses (12 to 14 dB in our frequency range at low temperature). The PNA is used as a MW source and allows transmission measurement. Furthermore, it is possible to gate the source using a pulse pattern generator (no pulsed experiments will be presented in this paper). A high field superconducting vector magnet is used to apply DC magnetic fields in ar-

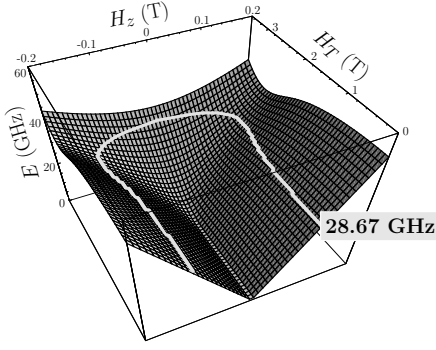


Figure 2: Energy separation E between the two lowest energy states $|A\rangle$ and $|S\rangle$ versus H_z and H_T . The locus of the resonance observed experimentally is a cut at constant energy, shown by the thick line.

bitrary directions with respect to the axes of the crystal.

To demonstrate the capabilities of our integrated sensor, we have studied $[\text{Ni}(\text{hmp})(\text{dmbCl})_4]$, henceforth referred to as Ni_4 . This is a particularly clean SMM with no solvate molecules present in its crystal phase and only 1% (natural abundance) of nuclear spins on the transition metal sites [13]. This results in narrower EPR peaks than in many SMMs [14]. The spin Hamiltonian of Ni_4 is to first approximation:

$$\mathcal{H} = -DS_z^2 - \mu_B \vec{H} \cdot \hat{g} \cdot \vec{S} + \mathcal{H}', \quad (1)$$

where the first term is the uniaxial anisotropy, the second the Zeeman energy, and the last one includes higher order anisotropy terms (*i.e.*, $-BS_z^4 + C(S_+^4 + S_-^4)$). The $S = 4$ ground state of the molecule at low temperature is the consequence of ferromagnetic exchange interactions between the four Ni^{II} ($S = 1$) ions. The uniaxial anisotropy leads to a large energy barrier $DS^2 \approx 12$ K (anisotropy field $H_a = 2DS/(g\mu_B) = 4.5$ T) to magnetization reversal between states of projection $S_z = \pm 4$ along the easy axis of the molecules (z). The two lowest energy states are the symmetric ($|S\rangle$) and antisymmetric ($|A\rangle$) linear combinations of $|up\rangle$ and $|down\rangle$ states. In the presence of a transverse field H_T , the latter are tilted away from the easy axis and have opposite z projections [7]. There is an energy separation between $|A\rangle$ and $|S\rangle$, known as the tunnel splitting Δ , which, in the field range in these experiments, increases with H_T when H_z equals zero. This energy separation also increases with H_z due to the Zeeman term. Thus, when a sample is irradiated at constant frequency f with a MW field h_{ac} aligned with z , it is possible to induce transitions between $|A\rangle$ and $|S\rangle$ and to map out the constant energy splitting ($= hf$) locus in the (H_z, H_T) phase space (*cf.* Fig. 2). These measurements enable determination of the spin-Hamiltonian parameters and set a lower bound of the decoherence time, as shown below. The transition rate is given by

the Fermi golden rule:

$$\Gamma = \frac{\pi}{2} \left(\frac{g\mu_B}{\hbar} h_{ac} \right)^2 |\langle S|S_z|A\rangle|^2 f(\omega) \quad (2)$$

where $\langle S|S_z|A\rangle$ is the matrix element coupling the states and $f(\omega)$ is a lorentzian of linewidth $1/T_2$.

In steady state, the absorbed power is simply $P_{abs} = \Gamma \hbar f n_d$, where n_d is the difference in population between states $|A\rangle$ and $|S\rangle$. When these states have different projections on the z -axis, the photon-induced transitions lead to a change in magnetization ΔM . If these projections on the z -axis are opposite, one can deduce ΔM from energy conservation. It is simply linked to the absorbed power and to the energy relaxation time T_1 [15]:

$$T_1 P_{abs} = \frac{\hbar f \Delta M N_0}{2M_{eq}}, \quad (3)$$

where N_0 and M_{eq} are the difference in population between $|A\rangle$ and $|S\rangle$ and the magnetization in the absence of MW, respectively. Thus, simultaneous measurements of P_{abs} and ΔM yield T_1 . We emphasize that this latter may be different from the spin-phonon relaxation time, as in the case of the phonon bottleneck [16, 17].

At the temperatures used in our experiments only the two lowest lying spin-levels are thermally populated. Moreover, for the transverse fields used, the thermal energy is smaller than the photon energy, $k_B T < \hbar f$. A pyramidal Ni_4 crystal is placed with one of its faces parallel to the plane of the sensor, in the middle of the microstrip resonator, and oriented so that h_{ac} is aligned with z , along the axis of the pyramid. The Hall device responds to the average magnetic field perpendicular to the plane of the sensor, which for the sample shape and placement, is mainly due to the z -component of the sample magnetization. Because of this pyramidal shape, the easy axis is not aligned ($\alpha = 20^\circ$) with H_L , which lies in the sensor plane. There is also a second misalignment $\theta < 5^\circ$ between H_L and the projection of the z axis on the sensor plane. The longitudinal field felt by the molecules is thus $H_z = H_L \cos \alpha \cos \theta + H_T \cos \alpha \sin \theta$, whereas the transverse field is to a good approximation H_T . Note that the EPR data are plotted versus H_z .

Fig. 3 presents the EPR signal measured at $f = 28.67$ GHz for several values of H_T as H_z is swept at 0.1 T/min. The power transmitted through the resonator is monitored in cw mode. The low power level used for this study induces a small increase of the sample temperature to 0.4 K. Two symmetric groups of peaks with respect to $H_z = 0$ T are observed. They correspond to transitions between $|A\rangle$ and $|S\rangle$. A multiple-lorentzian fit leads to two main peaks, A and B, assigned to two species of Ni_4 molecules present in the crystal, associated with different molecular environments [14]. As H_T is increased, the amplitude of the peaks increases and the resonance occurs at smaller H_z . As expected the

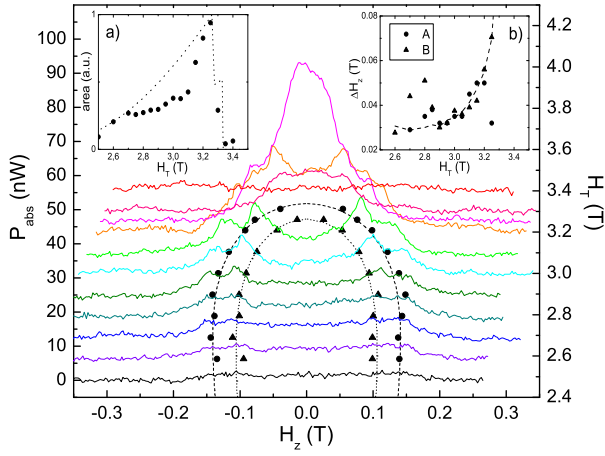


Figure 3: EPR absorption signal vs. longitudinal field H_z for several transverse fields H_T . $f = 28.67$ GHz, $P_{in} = 2.5$ μ W and $T = 0.4$ K. The circles and triangles denote the position of resonances. The dashed lines are the result of a direct diagonalization of \mathcal{H} . Insets: (a) integrated area under the EPR signal vs. H_T (b) linewidth of peaks A and B vs. H_T .

EPR signal disappears at large H_T as Δ becomes larger than hf . A direct diagonalization of \mathcal{H} yields the dependence of the energy splitting on H_z and H_T . The dashed line is a fit of the peak A data (circles) using $D_A = 0.757$ K, $B = 7.9 \cdot 10^{-3}$ K, $C = 3.25 \cdot 10^{-5}$ K, $g_z = 2.3$, $g_x = g_y = 2.23$. These parameters are in good agreement with high frequency cavity EPR measurements [14]. The dotted line is the best fit for peak B (triangles), obtained for $D_B = 0.785$ K, $B = 9.9 \cdot 10^{-3}$ K, $C = 3.25 \cdot 10^{-5}$ K, $g_z = 3.02$, $g_x = g_y = 2.39$. An extremely high value (unphysical) of g_z is needed to fit the data points, which is not understood at present.

The curvature of the energy splitting as the longitudinal field goes to zero is evidence of level repulsion, as already noted in ref. [7]. EPR has the advantage that one can measure the splitting at small H_z , where no or only small changes in the magnetization are expected. The inset (a) of Fig. 3 shows the area under the experimental absorption curves versus H_T . The dashed line is the prediction from the direct diagonalization of \mathcal{H} and Eq. 2. The calculation shows some discrepancy with the data in the intermediate regime of H_T . Nevertheless, it reproduces well the global behavior: the signal increases with H_T until peak B first disappears, followed by peak A. Using a semi-classical model (strictly valid for $S \gg 1$), an analytical expression for the linewidth of the EPR signal measured as H_z is swept can be obtained:

$$\Delta H_z = \frac{hf\delta E}{(2g\mu_B S_z^0)^2 H_z} \quad (4)$$

where δE is the energy broadening of the two levels and $S_z^0 = S\sqrt{1 - (H_T/H_a)^2}$. The dashed line in the inset (b) of Fig. 3 is a fit of the data with respect to δE . The fitting value corresponds to a transverse relaxation time

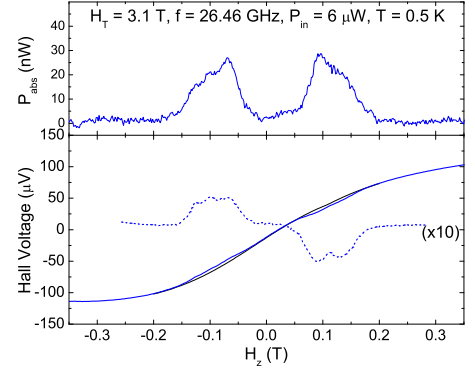


Figure 4: EPR signal (top) and photon-induced changes in the magnetization (bottom) of a Ni_4 crystal. The thin line is the equilibrium magnetization curve (MW off) and the dashed line the difference of magnetization curves with MW on and off expanded by a factor 10. The current in the Hall sensor was 10 μ A.

of 0.2 ns. This should be viewed as a lower bound of the decoherence time, $T_2 > 0.2$ ns, which is consistent with ref. [7]. We emphasize that no photon induced changes in the magnetization have been observed on this crystal, either at that low MW power, or in higher power pulsed MW experiments. Using Eq. 3, one can then deduce an upper bound for T_1 of 500 μ s, *i.e.* much less than it had been found in ref. [7].

Fig. 4 presents the EPR signal and the simultaneous measured changes in the magnetization of a different crystal than reported in Fig. 3. The same EPR spectroscopy study as that described above yields similar results. However in that case, there is a clear evidence of changes in the magnetization, at a similar level of absorbed power. This is due to a much longer T_1 , found to be 30 ms assuming that the same part of the crystal contributes to the signals measured by the Hall sensor and the PNA. We note that using the calibrated MW field strength, $h_{ac} = 9.8 \pm 1.5$ mOe, the estimation from the transition rate (Eq. 2) yields a power absorbed 30 times larger than that observed. One can thus infer that only 3% of the crystal is absorbing energy at the maximum of the resonance. We attribute that to inhomogeneous broadening of the absorption line.

In conclusion, simultaneous measurements of magnetization and EPR spectroscopy on tiny SMM single crystals have been demonstrated using an integrated sensor. The obtained EPR data are well explained using a direct diagonalization of the Hamiltonian of the spin system. Associated photon-induced changes in the magnetization depend on the energy relaxation time. The latter is seen to vary greatly between different crystals. This is probably linked to the thermalization of the crystal [17]. A detailed study of such effects is in progress. Finally, the integrated sensors developed for this work are also promising to conduct Rabi and spin-echo experiments.

Such experiments and real-time measurement of the magnetization should allow measurements of the intrinsic decoherence time and relaxation times in SMMs.

This work was supported by NSF (Grant No. DMR-0506946).

-
- [1] E. M. Chudnovsky et al., Phys. Rev. B **72**, 094426 (2005).
 - [2] M. N. Leuenberger and D. Loss, Nature **410**, 789 (2001).
 - [3] J. R. Friedman et al., Phys. Rev. Lett. **76**, 3830 (1996).
 - [4] L. Thomas et al., Nature **383**, 145 (1996).
 - [5] W. Wernsdorfer and R. Sessoli, Science **284**, 133 (1999).
 - [6] S. Hill et al., Science **302**, 1015 (2003).
 - [7] E. del Barco et al., Phys. Rev. Lett. **93**, 157202 (2004).
 - [8] W. Wernsdorfer et al., Phys. Rev. B **72**, 060409 (2005).
 - [9] A. Ardavan et al., quant-ph/0609143 (2006).
 - [10] E. M. Chudnovsky and D. A. Garanin, Phys. Rev. Lett. **89**, 157201 (2002).
 - [11] K. Gupta et al., *Microstrip Lines and Slotlines* (Artech House, 1996).
 - [12] A. D. Kent et al., J. Appl. Phys. **76**, 6656 (1994).
 - [13] E.-C. Yang et al., Polyhedron **22**, 1727 (2003).
 - [14] R. S. Edwards et al., J. Appl. Phys. **93**, 7807 (2003).
 - [15] N. Bloembergen and S. Wang, Phys. Rev. **93**, 72 (1954).
 - [16] A. Abragam and A. Bleaney, *Electron Paramagnetic Resonance of Transition Ions* (Clarendon Press, Oxford, 1970).
 - [17] D. A. Garanin, cond-mat/0609379 (2006).